Using the Varimax Norm method to enhance and identify edges of potential field data

Jiayong Yan [1,2,3] , *Zhihui Wang* [1,2] , *Fan Luo* [1,3] , *Chong Zhang* [1,2] ,
Yongqian Zhang [1,2] *and Xu Wang* [1,2]

[1] Chinese Academy of Geological Sciences, Beijing, China

[2] China Deep Exploration Center, China Geological Survey & Chinese Academy
of Geological Sciences, Beijing, China

[3] School of Geophysics and Measurement-control Technology, East China University
of Technology, Nanchang, Jiangxi, China

Edges detection and enhancement techniques of potential field data (gravity and magnetic data) are useful tools for finding the locations of anomalies at depth.Recently, these methods, including derivative-based filters, local phase filters and statistics-based techniques, have been increasingly widely used in solving geology problems, such as identifying subsurface faults, contacts, and other tectonic features. Nevertheless, general methods may not provide meaningful results for potential field data with heavy noise. To overcome these disadvantages, we present a new method named Varimax Norm (VariNorm) with a moving window to estimate the location of potential field data. Tests performed on the synthetic and field data in Tonling ore district show that the method does not require horizontal or vertical derivative calculations of any order, resists noise in nature and outperforms other traditional methods in a strong noise environment.

Keywords: edge enhancement, potential field, varimax norm, Tongling ore district

1. Introduction

Lots of methods for edge detection and enhancement are widely applied to potential field data(gravity and magnetic data) to distinguish between geological bodies with different densities and magnetic properties detailedly indicate subsurface faults, plutons, contacts, and other tectonic features (Alamdar et al., 2009; Sun et al., 2016). Among all the edge-detection methods, derivative-based filters have primarily and successfully been used to enhance short-wavelength anomalies produced by small and shallow sources; moreover, these methods are

simple to implement and are not computationally demanding (Hidalgo-Gato and Barbosa, 2015; Oliveira et al., 2017). The horizontal derivative enhances edges, whereas the vertical derivative narrows the width of anomalies (Cooper and Cowan, 2004). The most popular method is the total horizontal derivative (THD) filter. Guo et al. (2015) presented a hybrid positive-and-negative curvature approach for the detection of edges of magnetic anomalies. Roest et al. (1992) presented a new magnetic interpretation method based on the generalization of the analytic signal concept (AS).

However, the disadvantages of these derivative-based filters include their poor performance in the noisy data and poor-quality data and the tendency to enhance anomalies that are simultaneously produced by shallow bodies (Hidalgo-Gato and Barbosa, 2015). Local phase filters (edge enhancement methods) based on the phase variation of the derivative quantities have the advantage of flexibly producing new filters with the most applicability with only partial variation. (Alamdar and Ansari, 2010). Mitášová and Hofierka (1993) introduced the profile curvature (CPR), and Cooper (2009) suggested using its zero contours for edge detection. Following these methods, the tilt angle (T), the total horizontal derivative of the tilt angle (THDR) and the theta map (Theta) were also introduced to identify and enhance edges of potential field data,successively (Miller and Singh, 1994; Verduzco et al., 2004; Wijns et al., 2005). Cooper and Cowan (2006) compared the results of the T, THDR and Theta filters and introduced several new phase-based filters that have better performance. Ansari and Alamdar (2012) combined the analytic signal filter and the tilt angle filter to create a new edge detection filter. Li (2013) used the power transformation and the exponential transformation of the theta map to recognize the source edges. Wang et al. (2013) developed a method of normalizing the vertical derivative using the characteristics of the inverse hyperbolic tangent function. Li et al. (2014) improved the normalized horizontal tilt angle, local phase filter and theta map. Arısoy and Dikmen (2015) used the phase-adapted fractional-order horizontal derivative and vertical derivative of THD and AS. Oliveira et al. (2017) proposed an algorithm to estimate the depth and width of dyke-like magnetic sources based on normalized vertical and total horizontal derivatives.

Other methods are based on mathematical statistics. Among them, the most popular is known as the normalized standard deviation (NSTD) proposed by Cooper and Cowan (2008). Ma et al. (2012), Wang et al. (2012), Zhang et al. (2014) and Xu et al. (2015) also proposed methods based on statistics to detect edges in potential-field data. Additionally, Sun et al. (2016) outlined a method of developing the spectral-moment method.

In this paper, we present a new method based on the varimax norm (VariNorm). As implemented in the synthetic model, the VariNorm algorithm does not have to calculate the horizontal or vertical derivative of any order and can resist noise in nature using a moving window, and the process is more effective than that of other methods. Subsequently, this technique is applied to estimate

the edges of the sources from gravity anomalies and aeromagnetic anomalies in the Tongling ore district and its adjacent area. The results of the application provide an additional indicator for copper and gold deposit exploration.

2. Methodology

The varimax norm was first introduced and applied to indicate "spikiness" by Wiggins (1978), and it served as the core of minimum entropy deconvolution in seismic data processing. Subsequently, Levy and Oldenburg (1987) used VariNorm for zero-phase correction, and Fomel et al. (2007) further used it to focus on different diffraction events. The equation is defined as follows:

$$VariNorm = \frac{N \sum_{i=1}^{N} f_i^4}{(\sum_{i=1}^{N} f_i^2)^2} , \tag{1}$$

where f_i denotes the ith sample of the potential field data in the calculated window, and N represents the number of gravity or magnetic field data in the moving window. Equation 1 can also be interpreted as the inverse of the squared correlation coefficient between f^2 and 1 (Fomel et al., 2007):

$$VariNorm = \frac{1}{c(f^2,1)^2} , \tag{2}$$

where $c[f^2, 1]$ represents the correlation coefficient of

$$c\left[f^2,1\right] = \frac{\sum_{i=1}^{N} f_i^2}{\sqrt{N \sum_{i=1}^{N} f_i^4}} . \tag{3}$$

The varimax norm has a high value when the calculated window is near an anomaly's edge. Therefore, we can use the maximum value of VariNorm to identify and enhance the edges of potential field data.

3. Synthetic model test

A cubic body with top depth of 0.5 km is used to test this method. The size of the cubes is 40 km × 40 km × 40 km, and the density contrast is 0.5 g/cm^3. The synthetic data are calculated on a grid of 1001 × 1001 points, with a space of 0.1 km.

To verify the validity of this method, the results of the THD, C$_{PR}$, AS, T, THDR, Theta, NSTD, SECGGT, TAHG and ILP methods are compared with the VariNorm results (Figs. 1 and 2). The mathematical expressions are provided in

the appendix, and Figs. 1 and 2 show the results of the modelling and different edge detection filters without noise and with 1% random noise, respectively. As illustrated in Fig. 1, all edge detection filters can retrieve the horizontal view of the cube and locate the source bodies accurately.

Noise-free data represent an ideal assumption because all geophysical data are corrupted to some extent by noise. To test our method in a noisy environment, we add 1% random noise (Eq. 4) to the synthetic data and implement the same filters that were used with the noise-free data.

$$g = g + (g_{\max} - g_{min}) \times 0.01 \times randn(size(g)), \tag{4}$$

where g represents gravity data, *randn* is a function from the MATLAB that generates a matrix containing pseudorandom values drawn from the standard normal distribution. The results are shown in Fig. 2. Compared with Fig. 1, some of the results of the edge detection filters are blurred by noise, but the VariNorm result (Fig. 2l) still clearly gives the boundary of the cubic body.

4. Application to field data

To test the performance for field data of the VariNorm, we apply it to the gravity and aeromagnetic data from the Tongling ore district of east China, which is outlined in the red rectangle in Fig. 3.

The Tongling ore district located in the middle and lower reaches of the Yangtze River metallogenic belt is the most representative of large skarn metallogenic districts in the eastern China. The extracted minerals are mainly copper, iron, sulphur, gold, silver, lead and zinc (Yan et al., 2015). The regional stratigraphy consists of from Silurian to Quaternary stratigraphy except for the Lower and Middle Devonian. The northern and southern boundaries of the Tongling ore district are buried faults with an E-W trend, and the NE-trending large fault zone controls the boundaries of the east and west. The tectonic settings are overlaid by different tectonic directions and deformation characteristics, and develop the five group main structures, with NE, E-W, NNE, N-S and NW trends (Tang et al., 2013). In this area, the magmatism was very strong. There are about more than 70 small plutons exposed, which are mostly in the middle-shallow facies of small rock masses, rock branches or dikes, and the denudation degree is shallow. Theisotope dating results show that intrusive rocks related to mineralization mainly formed in the Late Jurassic (152-137Ma). The metal mineral resources of the Tongling ore districts are mainly concentrated in Tongguan Mountains, Shizi Mountains, Xinqiao, Fenghuang Mountains and Shatanjiao ore field, which are clustered along the Tonglin city to Daijiahui town basement fault zone, correspond to shallow plutons and are controlled by the same structures. The main ore deposits in these ore fields are distributed around the pluton, controlled by many groups of structures, and form the multilayer mineralization from the surface to depth. The mineralization is closely related to metallogenic
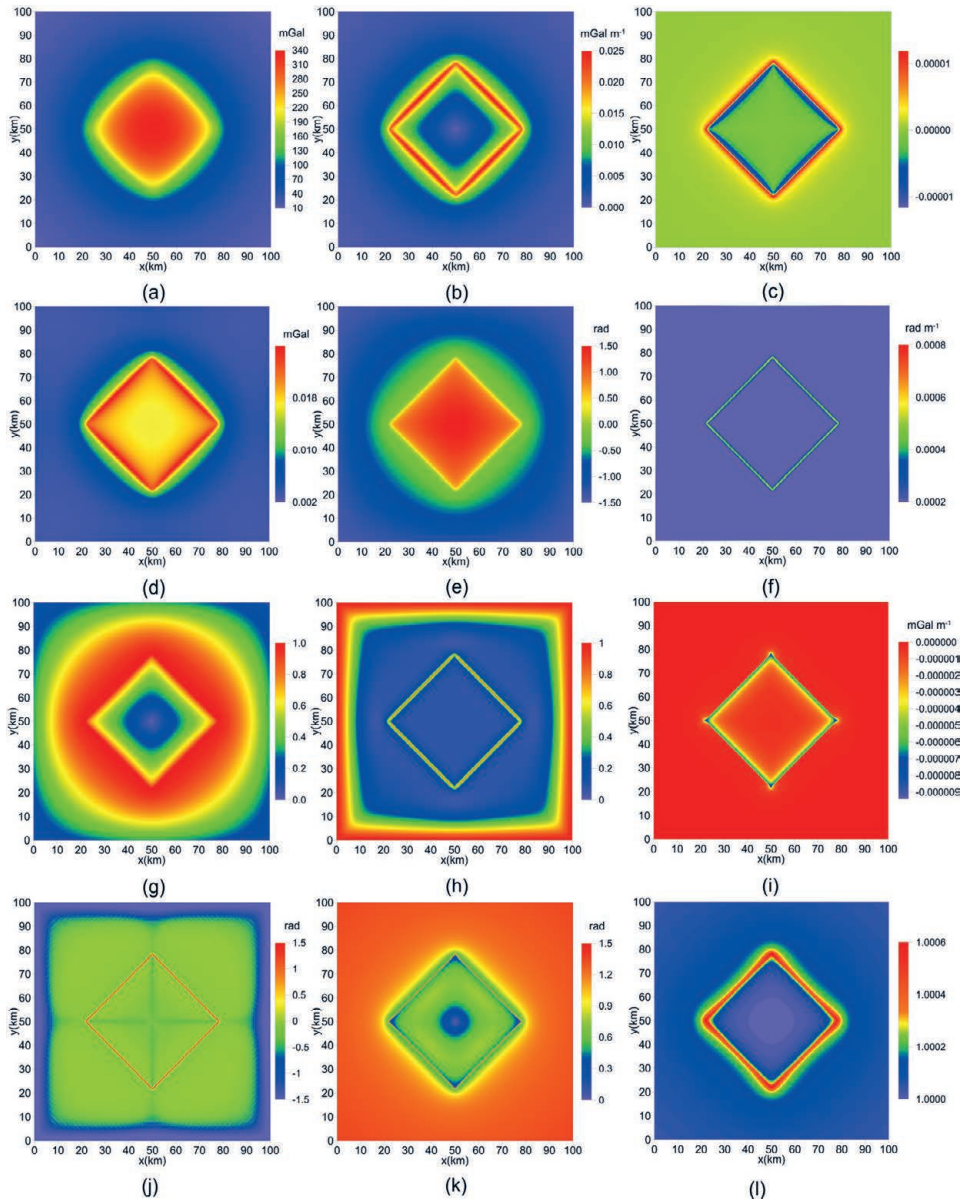
Figure 1. Applications of different edge detection filters on a cubic body with top depth of 0.5 km: (*a*) Synthetic gravity dataset (the white solid lines are the horizontal edges of the synthetic models), (*b*) THD results for the data in (*a*), (*c*) C$_{PR}$ results for the data in (*a*), (*d*) AS results for the data in (*a*), (*e*) T results for the data in (*a*), (*f*) THDR results for the data in (*a*), (*g*) Theta results for the data in (*a*), (*h*) NSTD results for the data in (*a*), (*i*) SECGGT results for the data in (*a*), (*j*) TAHG results for the data in (*a*), (*k*) ILP results for the data in (*a*), and (*l*) VariNorm results for the data in (*a*). A window size of 0.2 km × 0.2 km is used in (*h*) and (*l*).
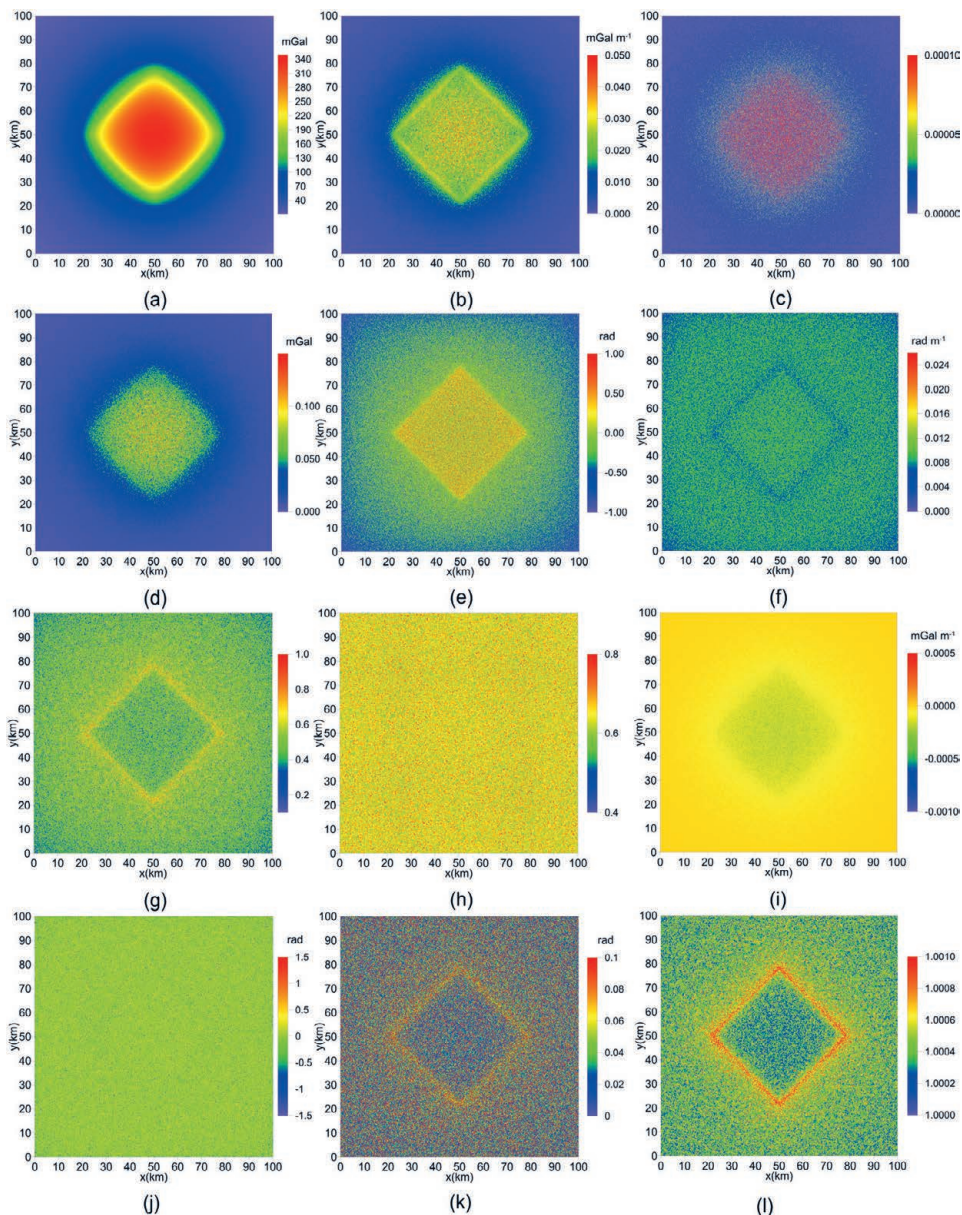
Figure 2. Test on noisy data: (*a*) Synthetic gravity data with 1% Gaussian noise, (*b*) THD results for the data in (*a*), (*c*) CPR results for the data in (*a*), (*d*) AS results for the data in (*a*), (*e*) T results for the data in (*a*), (*f*) THDR results for the data in (*a*), (*g*) Theta results for the data in (*a*), (*h*) NSTD results for the data in (*a*), (*i*) SECGGT results for the data in (*a*), (*j*) TAHG results for the data in (*a*), (*k*) ILP results for the data in (*a*), and (*l*) the VariNorm results for the data in (*a*). A window size of 0.2 km × 0.2 km is used in (*h*) and (*l*).
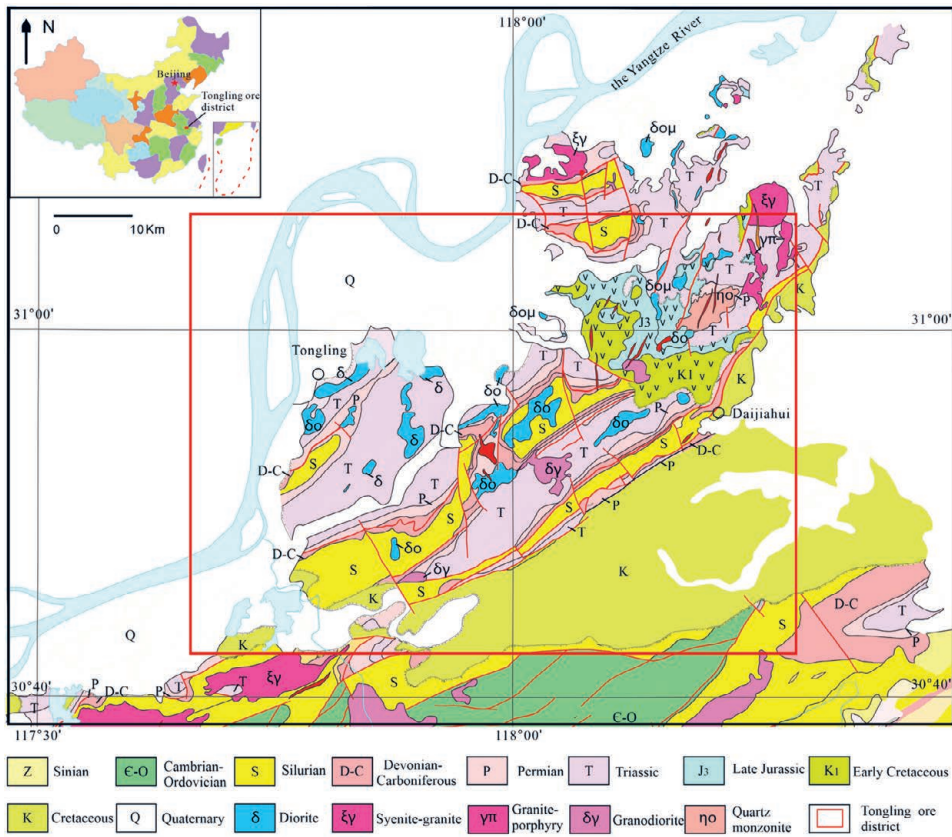
Figure 3. Regional geological setting of the Tongling ore district and its adjacent area (after Yan et al., 2015).

plutons, but more important is the composite control by the faults and magmatic activity in this area. Therefore, it is important for prospective targeting to detect the distribution of structures and plutons (Yan et al., 2015).

Figures 4 to 7 show the Bouguer gravity anomaly, aeromagnetic anomaly and different edge detection results, respectively. The Bouguer gravity anomaly (Fig. 4a) and aeromagnetic anomaly (Fig. 6a) both have a resolution of 500 m × 500 m, and they indicate that the regional structural trend is predominately oriented northeast and that several intrusive and extrusive rocks are distributed along the regional structural trend. However, the detailed structural characteristics and the edges of the intrusive and extrusive rocks cannot be identified. We processed the gravity and magnetic data using different edge detection methods, including the VariNorm method. In Figs. 4 and 5, different edge detection methods show different results in detail. THD, CPR, AS and T
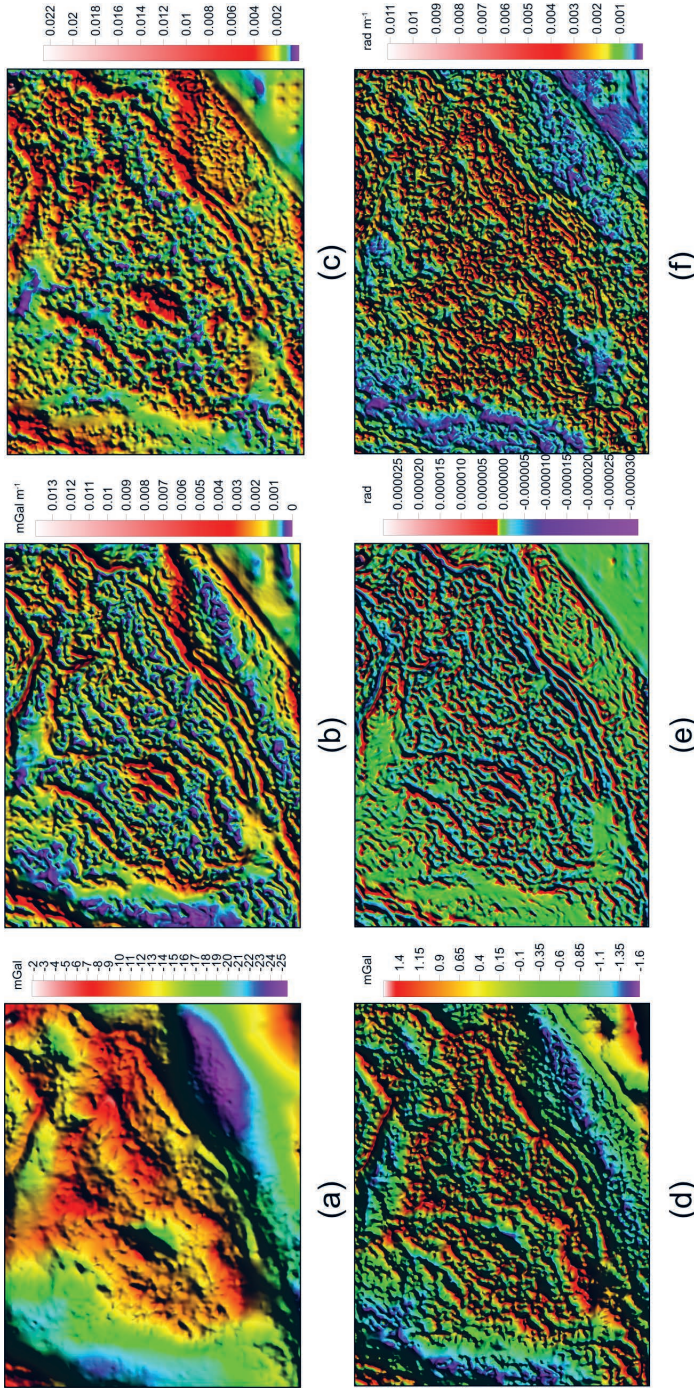
Figure 4. Bouguer gravity data and different edge detection and enhancement results over the Tongling ore district and its adjacent area. (*a*) Bouguer gravity data, (*b*) THD results for the data in (*a*), (*c*) CPR results for the data in (*a*), (*d*) AS results for the data in (*a*), (*e*) T results for the data in (*a*), (*f*) THDR results for the data in (*a*).
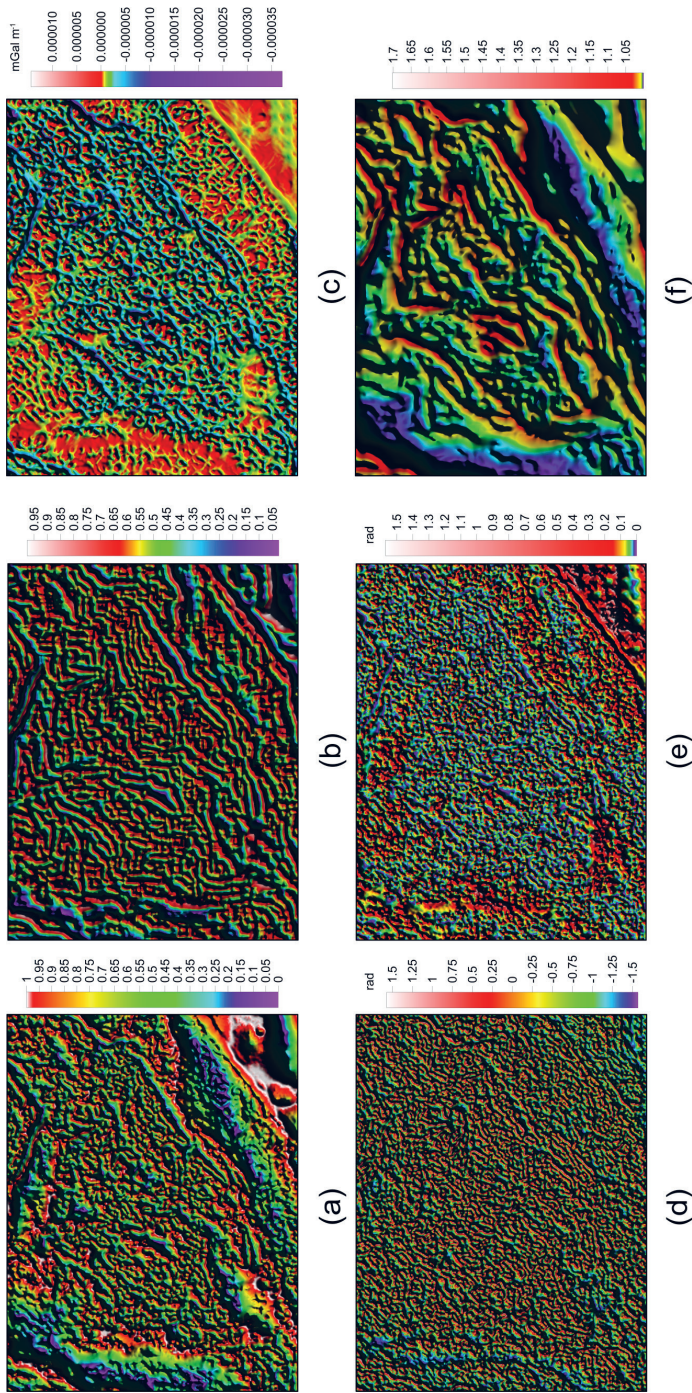
Figure 5. Different edge detection and enhancement results of Bouguer gravity data over the Tongling ore district and its adjacent area. (a) Theta results for the data in Fig. 4a, (b) NSTD results for the data in Fig. 4a, (c) SECGGT results for the data in Fig. 4a, (d) TAHG results for the data in Fig. 4a, (e) ILP results for the data in Fig. 4a, and (f) the VariNorm results for the data in Fig. 4a. A window size of 1000 m × 1000 m is used in (b) and (f)
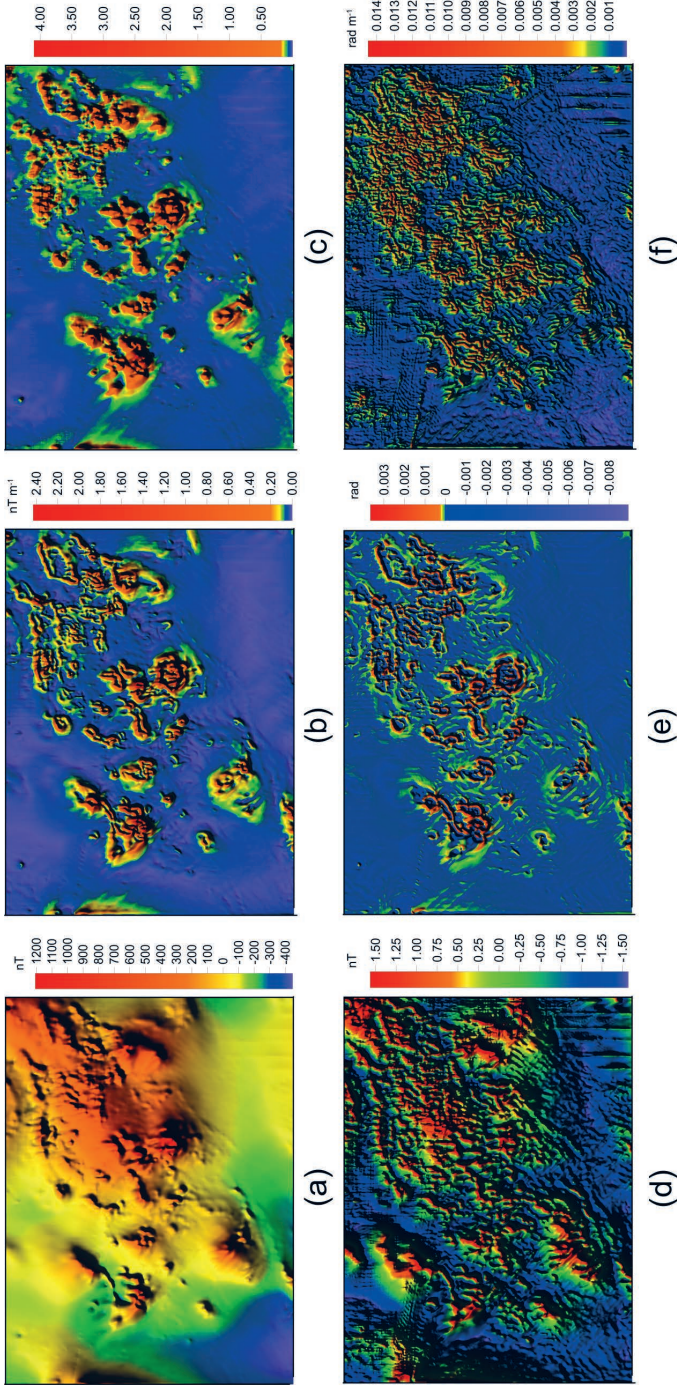
Figure 6. Results of aeromagnetic data and different edge detection and enhancement results over the Tongling ore district and its adjacent area. (*a*) Aeromagnetic anomalies, (*b*) THD results for the data in (*a*), (*c*) CPR results for the data in (*a*), (*d*) AS results for the data in (*a*), (*e*) T results for the data in (*a*), (*f*) THDR results for the data in (*a*).
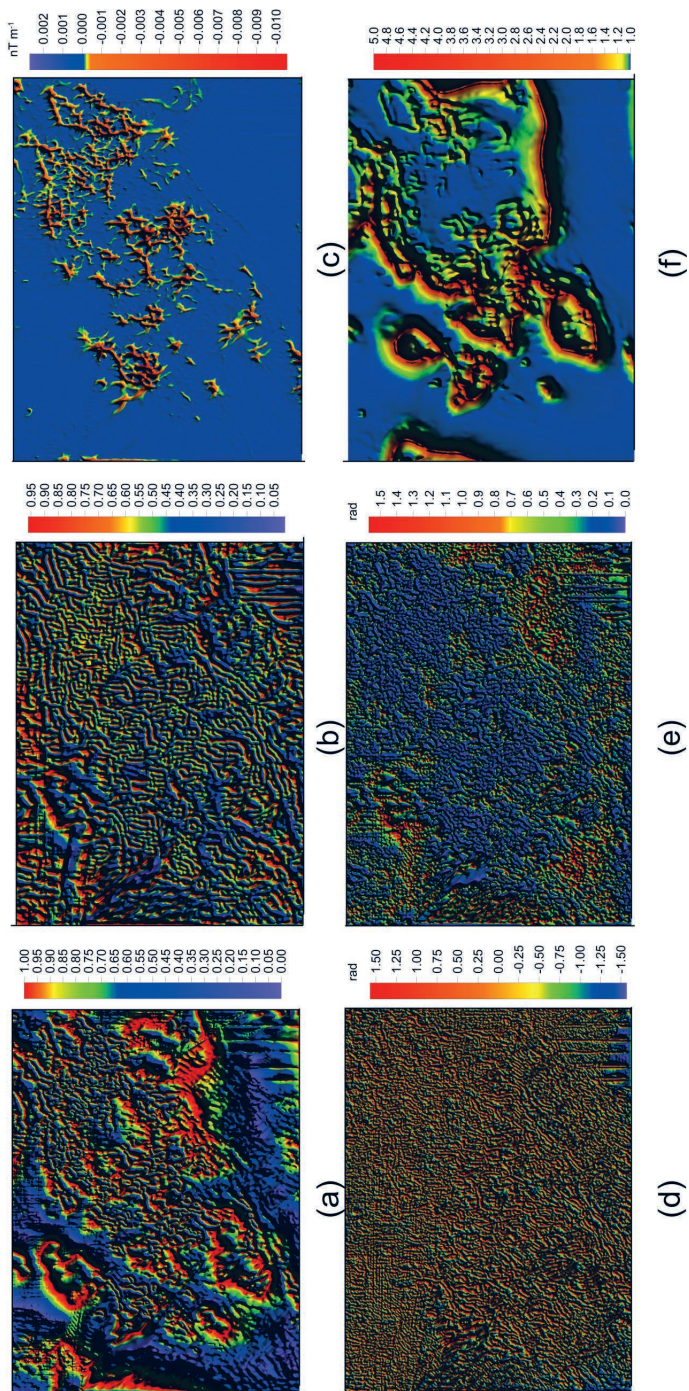
Figure 7. Different edge detection and enhancement results of aeromagnetic data over the Tongling ore district and its adjacent area. (*a*) Theta results for the data in Fig. 4a, (*b*) NSTD results for the data in Fig. 4a, (*c*) SECGGT results for the data in Fig. 4a, (*d*) TAHG results for the data in Fig. 4a, (*e*) ILP results for the data in Fig. 4a, and (*f*) the VariNorm results for the data in Fig. 4a. A window size of 1000 m × 1000 m is used in (*b*) and (*f*).
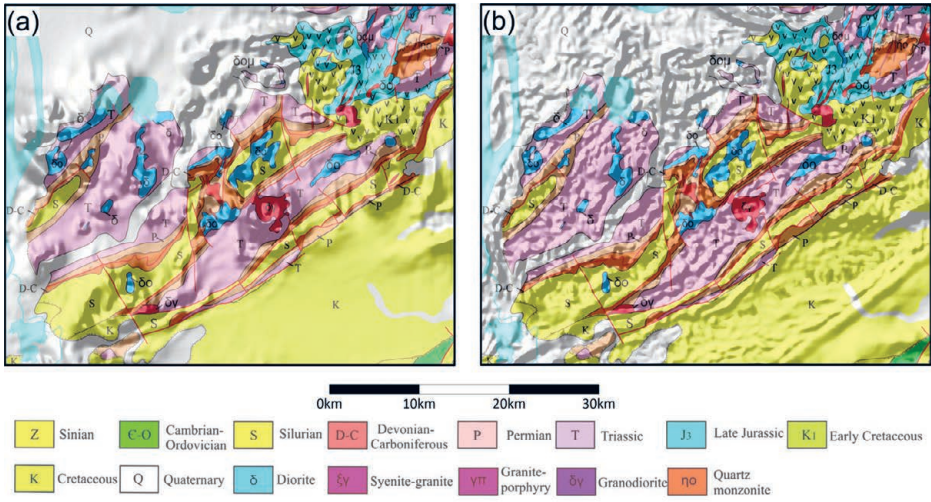
Figure 8. Comparison the VariNorm result of aeromagnetic (*a*) and gravity (*b*) data overlap geological map.

depict the regional structures, THDR, while Theta, NSTD and SECGGT depict more small-scale structures. It is difficult to recognize some geological information in TAHG and ILP. In Figs. 6 and 7, THD, CPR, T and Theta recognize the boundaries of intrusive rocks,while others cannot locate rocks. Compared with these methods, the results of VariNorm (Figs. 5f and 7f) also gave a performance not only in the regional but also in the local features. The improvements have helped geologists understand the geological setting and dynamic characteristics of the Tongling ore deposit and its adjacent area. The edges of gravity data showed faults and folds related to metallogenesis. The edges of the aeromagnetic data showed intrusive and extrusive rocks, which are favourable target areas for skarn-type copper and gold deposits.

To test the validity, the VariNorm results of aeromagnetic and gravity are overlaid with the geological map. As shown in Figs. 8a and 8b, the results correspond closely to outcrops and boundaries of rocks and faults that are buried in the Quaternary and Cretaceous basins.

5. Discussions

The results of synthetic and field data show that the VariNorm method is a useful tool to detect edges in potential field data. However, several parameters are vital for obtaining reliable results.

First, the window size is an important parameter used in the calculation. Small window sizes are helpful for delineating small amplitude anomalies but
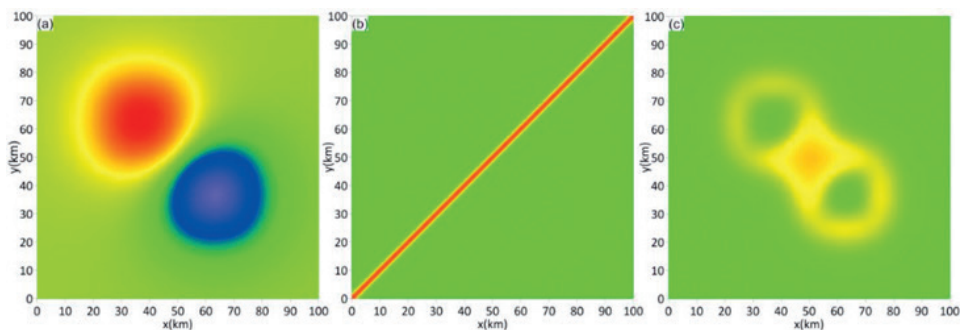
Figure 9. The results of two square blocks with the positive and negative densities, the gravity anomaly (*a*), the result of applying the VariNorm method directly, and the VariNorm result after a certain number to eliminate the zero contours.

generate discontinuities. In contrast, large window sizes help to delineate large-scale structures and rock body boundaries, and the results have good continuity, but small amplitude anomalies cannot be identified. As with other edge detection methods based on the window calculation (Cooper and Cowan, 2008), the suitable window size could be obtained by trying to choose different parameters to calculate the VariNorm.

Second, this method is sensitive to the boundary of positive and negative anomalies and usually does not work well. To solve this problem, we propose a useful method to improve it and give an example. The gravity anomalies of two square blocks with positive and negative density contrast are shown in Fig. 9a. Because of the zero contour of the Laplacian existing, the result (Fig. 9b) misses the two square bodies by applying the VariNorm method directly. To suppress the amplitude along the diagonal, we add a certain number to the gravity anomaly (Fig. 9a) to make the value far away from zero and then calculate it again. The two square blocks are located successfully (Fig. 9c).

6. Conclusions

In this paper, we present a new edge detection method, test it on synthetic and field data, and obtain acceptable results compared with traditional methods. The VariNorm method can enhance the edges of sources clearly and capture subtle details of potential field data. Because the VariNorm method does not have to calculate a horizontal or vertical derivative of any order, it can obtain a more reliable result when handling the noisy and poor-quality data.

References

Alamdar, K. and Ansari, A. H. (2010): Edge detection of potential field anomalies using local phase filters, *J. Earth Space Phys.,* **36**, 47–58.

Alamdar, K., Ansari, A. H. and Ghorbani, A. (2009): Edge detection of potential field anomalies using tilt angle and its inferred filters, *EGU General Assembly Conference: Abstract Series.* 19.

Ansari, A. H. and Alamdar, K. (2012): A new edge detection method based on the analytic signal of tilt angle (ASTA) for magnetic and gravity anomalies, *Iran. J. Sci. Technol. A*, **35**, 81–88, https://doi.org/10.22099/IJSTS.2011.2131.

Arısoy, M. Ö. and Dikmen, Ü. (2015): Edge enhancement of magnetic data using fractional-order-derivative filters, *Geophysics*, **80**, 7–17, https://doi.org/10.1190/geo2013-0473.1.

Cooper, G. R. J. (2009): Balancing images of potential field data, *Geophysics*, **74**, 17–20, https://doi.org/10.1190/1.3096615.

Cooper, G. R. J. and Cowan, D. R. (2004): Filtering using variable order vertical derivatives, *Comput. Geosci.*, **30**, 455–459, https://doi.org/10.1016/j.cageo.2004.03.001.

Cooper, G. R. J. and Cowan, D. R. (2006): Enhancing potential field data using filters based on the local phase, *Comput. Geosci.*, **32**, 1585–1591, https://doi.org/10.1016/j.cageo.2006.02.016.

Cooper, G. R. J. and Cowan, D. R. (2008): Edge enhancement of potential-field data using normalized statistics, *Geophysics*, **73**, 1–4, https://doi.org/10.1190/1.2837309.

Fomel, S. E., Landa, E. and Taner, M. T. (2007): Poststack velocity analysis by separation and imaging of seismic diffractions, *Geophysics*, **72**, 89–94, https://doi.org/10.1190/1.2781533.

Ferreira, F. J., de Souza, F. J., Bongiolo, A. B. S. and de Castro. L. G. (2013): Enhancement of the total horizontal gradient of magnetic anomalies using the tilt angle, *Geophysics*, **78**, 33–41, https://doi.org/10.1190/geo2011-0441.1.

Guo, L. H., Gao, R., Meng, X. H. and Zhang, G. L. (2015): A hybrid positive-and-negative curvature approach for detection of the edges of magnetic anomalies, and its application in the South China Sea, *Pure Appl. Geophys.*, **172**, 2701–2710, https://doi.org/10.1007/s00024-014-0956-y.

Hidalgo-Gato, M. C. and Barbosa, V. C. F. (2015): Edge detection of potential-field sources using scale-space monogenic signal: fundamental principles, *Geophysics*, **80**, 27–36, https://doi.org/10.1190/geo2015-0025.1.

Levy, S. and Oldenburg, D. W. (1987): Automatic phase correction of common-midpoint stacked data, *Geophysics*, **52**, 51–59, https://doi.org/10.1190/1.1442240.

Li, L. L. (2013): Improved edge detection tools in the interpretation of potential field data, *Explor. Geophys.*, **44**, 128–132, https://doi.org/10.1071/eg12058.

Li, L. L., Huang D, N., Han, L. and Ma, G. Q. (2014): Optimised edge detection filters in the interpretation of potential field data, *Explor. Geophys.*, **45**, 171–176, https://doi.org/10.1071/eg13059.

Ma, G. Q., Huang, D. N., Yu, P. and Li, L. L. (2012): Application of improved balancing filters to edge identification of potential field data, *Chinese Journal of Geophysics*, **55**, 4288–4295 (in Chinese).

Miller, H. G. and Singh, V. (1994): Potential field tilt – A new concept for location of potential field sources, *J. Appl. Geophys.*, **32**, 213–217, https://doi.org/10.1016/0926-9851(94)90022-1.

Mitášová, H. and Hofierka, J. (1993): Interpolation by regularized spline with tension: II Application to terrain modeling and surface geometry analysis, *Math Geol.*, **25**, 657–669, https://doi.org/10.1007/bf00893172.

Oliveira, S. P., Ferreira, F. J. F. and de Souza, J. (2017): An algorithm for automatic edge detection in potential field anomaly images – Application to dike-like magnetic structures, *Comput. Geosci.*, **103**, 80–91, https://doi.org/10.1016/j.cageo.2017.02.006.

Oruç, B., Sertçelik, I., Kafadar, Ö. and Selim, H. H. (2013): Structural interpretation of the Erzurum Basin eastern Turkey using curvature gravity gradient tensor and gravity inversion of basement relief, *J. Appl. Geophys.*, **88**, 105–113, https://doi.org/10.1016/j.jappgeo.2012.10.006.

Roest, W., Verhoef, R. J. and Pilkington, M. (1992): Magnetic interpretation using the 3-D analytic signal, *Geophysics*, **57**, 116–125, https://doi.org/10.3997/2214-4609.201410982.

Sun, Y., Yang, W., Zeng, X. and Zhang, Z. (2016): Edge enhancement of potential field data using spectral moments, *Geophysics*, **81**, 1–11, https://doi.org/10.1190/geo2014-0430.1.

Tang, J. T., Zhou, C., Wang, X. Y., Xiao, X. and Lü, Q. T. (2013): Deep electrical structure and geological significance of Tongling ore district, *Tectonophysics*, **606**, 78–96, https://doi.org/10.1016/j.tecto.2013.05.039.

Verduzco, B., Fairhead, J. D., Green, C. M. and MacKenzie, C. (2004): New insights into magnetic derivatives for structural mapping, *The Leading Edge*, **23**, 116–119, https://doi.org/10.1190/1.1651454.

Wang, M., Guo, Z. H., He, H. and Luo, F. (2013): Edge detection of potential field data using inverse hyperbolic tangent, *Geophys. Geochem. Explo.*, **37**, 665–663. (in Chinese with English abstract), https://doi.org/10.1071/eg12022.

Wang, Y. G., Wang, Z. W., Zhang, F. X., Zhang, J. Z., Tai, H. and Guo, C. C. (2012): Edge detection of potential field based on normalized vertical gradient of mean square error ratio, *J. China Univ. Petrol.*, **36**, 86–90 (in Chinese with English Abstract), https://doi.org/10.3969/j.issn.1673-5005.2012.02.014.

Wiggins, R. A. (1978): Minimum entropy deconvolution, *Geoexploration*, **16**, 21–35, https://doi.org/10.1016/0016-7142(78)90005-4.

Wijns, C., Perez, C. and Kowalczyk, P. (2005): Theta map: Edge detection in magnetic data, *Geophysics*, **70**, L39–L43, https://doi.org/10.1190/1.1988184.

Xu, M. C., Yang, Y., Wu, J. C. and Huan, H. (2015): Edge detection in the potential field using the correlation coefficients of multidirectional standard deviations, *Appl. Geophys.*, **12**, 23–34. https://doi.org/10.1007/s11770-014-0473-5.

Yan, J. Y., Lü, Q. T., Chen, M. C., Deng, Z., Qi, G., Zhang, K., Liu, Z. D., Wang, J. and Liu, Y. (2015): Identification and extraction of geological structure information based on multi-scale edge detection of gravity and magnetic fields an example of the Tongling ore concentration area, *Chinese Journal of Geophysics*, **58**, 4450–4464 (in Chinese with English Abstract), https://doi.org/10.6038/cjg20151210.

Zhang, H. L., Ravat, D., Marangoni, Y. R. and Hu, X. Y. (2014): NAV-Edge: Edge detection of potential-field sources using normalized anisotropy variance, *Geophysics*, **79**, 43–53, https://doi.org/10.1190/geo2013-0218.1.

SAŽETAK

Primjena Varimax Norm metode za poboljšanje i prepoznavanje rubnih podataka polja potencijala

Jiayong Yan, Zhihui Wang, Fan Luo, Chong Zhang, Yongqian Zhang i Xu Wang

Tehnike otkrivanja i poboljšanja rubova podataka potencijalnih polja (gravitacijski i magnetski podaci) korisni su alati za pronalaženje mjesta anomalija u dubini. Nedavno

su ove metode, uključujući filtre na bazi derivata, lokalne fazne filtre i tehnike temeljene na statistikama, sve više naširoko se koristi u rješavanju geoloških problema, poput identificiranja podzemnih rasjeda, kontakata i drugih tektonskih značajki. Ipak, opće metode možda neće pružiti značajne rezultate za potencijalne terenske podatke s jakom bukom. Da bismo prevladali ove nedostatke, predstavljamo novu metodu pod nazivom Varimax Norm (VariNorm) s pomičnim prozorom za procjenu mjesta potencijalnih podataka polja. Ispitivanja izvedena na sintetičkim i poljskim podacima u rudnom području Tonling pokazuju da metoda ne zahtijeva vodoravne ili okomite izračune izvedenih derivata bilo kojeg reda, odolijeva buci u prirodi i nadmašuje ostale tradicionalne metode u jakom okruženju buke.

Ključne riječi: poboljšanje ruba, polje potentijala, varimax norm, distrikt Tongling ore

Corresponding author's address: Zhihui Wang, Chinese Academy of Geological Sciences, No. 26 Baiwangzhuang Street, Xicheng District, 100037 Beijing, China; e-mail: wangzhihui1982@outlook.com

Appendix

Equations for the filters used in this study.

1. The horizontal derivative is defined as:

$$THD = \sqrt{\left(\frac{\partial f}{\partial x}\right)^2 + \left(\frac{\partial f}{\partial y}\right)^2} \; .$$

2. The total-gradient filter (Roest et al., 1992) is defined as:

$$AS = \sqrt{\left(\frac{\partial f}{\partial x}\right)^2 + \left(\frac{\partial f}{\partial y}\right)^2 + \left(\frac{\partial f}{\partial z}\right)^2} \; .$$

3. The tilt angle (Miller and Singh, 1994) is defined as:

$$T = \tan^{-1}\left(\frac{\dfrac{\partial f}{\partial z}}{\sqrt{\left(\dfrac{\partial f}{\partial x}\right)^2 + \left(\dfrac{\partial f}{\partial y}\right)^2}}\right) \; .$$

4. The profile curvature (Mitášová and Hofierka, 1993) is defined as:

$$C_{PR} = \frac{\dfrac{\partial^2 f}{\partial x^2}\left(\dfrac{\partial f}{\partial x}\right)^2 + 2\dfrac{\partial^2 f}{\partial x \partial y}\dfrac{\partial f}{\partial x}\dfrac{\partial f}{\partial y} + \dfrac{\partial^2 f}{\partial y^2}\left(\dfrac{\partial f}{\partial y}\right)^2}{p\sqrt{q^3}} \; ,$$

where $p = \left(\dfrac{\partial f}{\partial x}\right)^2 + \left(\dfrac{\partial f}{\partial y}\right)^2$.

5. The total horizontal derivative of the tilt angle (Verduzco et al., 2004) is defined as:

$$THDR = \sqrt{\left(\frac{\partial f}{\partial x}\right)^2 + \left(\frac{\partial f}{\partial y}\right)^2} \; .$$

6. The theta map (Wijns et al., 2005) is defined as:

$$Theta = \frac{\sqrt{\left(\dfrac{\partial f}{\partial x}\right)^2 + \left(\dfrac{\partial f}{\partial y}\right)^2}}{\sqrt{\left(\dfrac{\partial f}{\partial x}\right)^2 + \left(\dfrac{\partial f}{\partial y}\right)^2 + \left(\dfrac{\partial f}{\partial z}\right)^2}} \; .$$

7. The ratio of the related normalized standard deviations (Cooper and Cowan, 2008) is defined as:

$$NSTD = \frac{\sigma\left(\frac{\partial f}{\partial z}\right)}{\sigma\left(\frac{\partial f}{\partial x}\right) + \sigma\left(\frac{\partial f}{\partial y}\right) + \sigma\left(\frac{\partial f}{\partial z}\right)},$$

where σ represents the standard deviations computed in the moving window.

8. The SECGGT method (Oruç et al., 2013) uses the smaller of the two eigenvalues from the CGGT and is defined as:

$$SECGGT = \frac{1}{2}\left(\frac{\partial f_x}{\partial x} + \frac{\partial f_y}{\partial y} - \sqrt{\left(\frac{\partial f_x}{\partial x} - \frac{\partial f_y}{\partial y}\right)^2 + 4\left(\frac{\partial f_x}{\partial y}\right)^2}\right),$$

$$SECGGT = \begin{pmatrix} \dfrac{\partial f_x}{\partial x} & \dfrac{\partial f_x}{\partial y} \\ \dfrac{\partial f_y}{\partial x} & \dfrac{\partial f_y}{\partial y} \end{pmatrix},$$

where f_x and f_y are the horizontal vectors of the potential field f. The zero value delineates the source edges.

9. The TAHG (Ferreira et al., 2013) is defined as:

$$TAHG = \tan^{-1}\left(\frac{\dfrac{\partial THDR}{\partial z}}{\sqrt{\left(\dfrac{\partial THDR}{\partial x}\right)^2 + \left(\dfrac{\partial THDR}{\partial y}\right)^2}}\right).$$

10. The improved local phase filter (Ma, 2013) uses a combination of the first-order horizontal and second-order horizontal derivatives to recognize source edges, which can be expressed as:

$$ILP = \sin^{-1}\left[\frac{\sqrt{\left(\dfrac{\partial f}{\partial x}\right)^2 + \left(\dfrac{\partial f}{\partial y}\right)^2}}{\sqrt{\left(\dfrac{\partial f}{\partial x}\right)^2 + \left(\dfrac{\partial f}{\partial y}\right)^2 + \left(\left(\dfrac{\partial^2 f}{\partial^2 x} + \dfrac{\partial^2 f}{\partial^2 y}\right) \cdot \dfrac{mean(\partial f / \partial z)}{mean(\partial^2 f / \partial z^2)}\right)^2}}\right].$$